INL/JOU-20-57871-Revision-0

Density Functional Theory Study of the Initial Stages of Cl-Induced Degradation of a-Cr2O3 Passive Film

September 2020

Kofi Sarfo, Pratik Murkute, Melissa Santala, Yongfeng Zhang, Julie Tucker, Lney rnadttir

Changing the World's Energy Future

INL is a U.S. Department of Energy National Laboratory operated by Battelle Energy Alliance, LLC

INL/JOU-20-57871-Revision-0

Density Functional Theory Study of the Initial Stages of Cl-Induced Degradation of a-Cr2O3 Passive Film

Kofi Sarfo, Pratik Murkute, Melissa Santala, Yongfeng Zhang, Julie Tucker, Lney rnadttir

September 2020

Idaho National Laboratory
Idaho Falls, Idaho 83415

http://www.inl.gov

Prepared for the
U.S. Department of Energy
Under DOE Idaho Operations Office
Contract DE-AC07-05ID14517

Journal of The Electrochemical Society

Density Functional Theory Study of the Initial Stages of Cl-Induced Degradation of α-Cr_2O_3 Passive Film

Journal of The Electrochemical Society, 2020 **167** 121508

Density Functional Theory Study of the Initial Stages of Cl-Induced Degradation of α-Cr_2O_3 Passive Film

Kofi Oware Sarfo,[1] Pratik Murkute,[2] O. Burkan Isgor,[2] Yongfeng Zhang,[3,4] Julie Tucker,[5] and Líney Árnadóttir[1,*,z]

[1]*School of Chemical, Biological, and Environmental Engineering, Oregon State University, Corvallis, Oregon 97331, United States of America*
[2]*School of Civil and Construction Engineering, Oregon State University, Corvallis, Oregon 97331, United States of America*
[3]*Engineering Physics Department, University of Wisconsin-Madison, Wisconsin 53711, United States of America*
[4]*Idaho National Laboratory, Idaho Falls, Idaho 83401, United States of America*
[5]*School of Mechanical, Industrial and Manufacturing Engineering, Oregon State University, Corvallis, Oregon 97331, United States of America*

The ion exchange and point defect models are two prominent models describing the role of anions, such as chlorides, in the degradation of passive oxide films. Here the thermodynamic feasibility of critical steps of Cl-induced degradation of a hydroxylated α-Cr_2O_3 (0001) surface, as proposed by these two models, are studied. Both models begin with Cl substitution of surface OH and H_2O, which becomes less favorable with increasing Cl coverage. The initial stages of Cl-induced breakdown of the α-Cr_2O_3 depend on Cl coverage and the presence of O vacancy near the surface as follows: (1) neither Cl insertion (supporting the ion exchange model) nor Cr vacancy formation (supporting the point defect model) is feasible at low Cl coverages except in the presence of O vacancies near the surface, where Cl insertion is thermodynamically feasible even at low coverages, (2) in the absence of O vacancies, Cr vacancy formation becomes feasible from 10/12 ML onwards whereas Cl insertion by exchange with subsurface OH only becomes feasible at full coverage. This implies that at higher coverages Cl-induced degradation first initiatesthrough a vacancy formation mechanism, but both insertion and vacancy formation would be feasible at full coverage.
 [DOI: 10.1149/1945-7111/abb381]

Manuscript submitted June 2, 2020; revised manuscript received August 25, 2020. Published September 9, 2020. *This was paper 1001 presented at the Dallas, Texas, Meeting of the Society, May 26, 2019–May 30, 2019.*

Supplementary material for this article is available online

The corrosion resistance of stainless steel has been attributed to the presence of a protective Cr-enriched (α-Cr_2O_3) passive layer that protects the metal surface from active corrosion.[1–4] The exposure of the protective layer to aggressive ions like chlorides can lead to a breakdown of the passive film and pitting.[5] Understanding the surface chemistry on these oxide surfaces in different exposure conditions provides an essential insight into the stability and functionality of the protective layers. Although there is a general consensus that chlorides play a significant role in the depassivation and pitting of stainless steel, the molecular mechanism and the role of chlorides in these processes is still debated.[6–10]

Two widely applied models for breakdown of the passive film, the ion exchange and the point defect models are illustrated in Fig. 1. According to the ion exchange model, pit initiation in chloride-containing solutions involves chloride adsorption, chloride insertion by ion exchange with subsurface O or into an O vacancies, and migration through the oxide film, leading to localized metal dissolution at the metal/film interface.[5,11] The ion exchange model is supported by experimental studies suggesting the presence of chlorides inside the oxide film.[12–16] For example, chloride has been detected, inside an Al_2O_3 passive layer of an Al alloy exposed to 0.1 M NaCl solution using X-ray photoelectron spectroscopy (XPS),[17] and at the passive film and the metal/film interface of an $FeCr_{15}Ni_{15}$ alloy exposed to 0.3 M NaCl solution using super X-ray energy-dispersive spectrometer.[14] Subsurface Cl has also been proposed to be thermodynamically feasible by density functional theory (DFT) calculations of defect-free hydroxylated NiO (111) at high Cl coverage.[18]

Unlike the ion exchange model, in the point defect model, the chlorides are not inserted into the passive film but act as a catalyst for cation vacancy formation on the surface.[16,19–21] The cation vacancies then migrate to the metal/film interface and oxidize the metal at the interface. If the rate of cation vacancies entering the metal phase is lower than the rate of cation vacancies migrating to the metal/film interface, the cation vacancies accumulate locally at the metal/film interface and form a void. The local detachment of the film in the void region leads to stress and subsequent breakdown of the passive film.[20,21] This model is supported by a range of experimental studies showing the dissolution of metal cation as chloride salts from the passive film leaving behind cation vacancies.[23–25]

The use of computational methods, like DFT, to study Cl interactions with oxide surfaces has been critical in the molecular understanding of the ion exchange and point defect models showing how the mechanisms vary between oxides. For example, DFT calculations of Cl insertion by exchange with subsurface oxygen (in support of the ion exchange model) was found to be favorable at high Cl coverages on NiO (111),[18,26] but for α-Fe_2O_3, iron surface vacancy formation (in support of the point defect model) was more favorable than Cl insertion.[24,27–30]

Here we use DFT to study the Cl interactions with a hydroxylated α-Cr_2O_3 (0001) surface and bulk oxide. Our discussion focuses on the two characteristic steps of the ion exchange and point defect models, Cl insertion and Cl-induced Cr vacancy formation, and provides a new understanding of the initial stages of degradation of α-Cr_2O_3 passive film.

Method

Computational details.—All calculations are based on DFT as implemented in the Vienna Ab Initio Simulation Package (VASP)[31–34] using generalized gradient approximation (GGA) with the Perdue-Burke-Erzerhof (PBE) exchange-correlation functional.[35] Electron-ion interactions were described using the projector augmented wave (PAW) potential,[36,37] and plane wave basis set with 520 eV cut off energy was used for all calculations. A 3 × 3 × 1 Monkhorst-Pack *k-point* sampling was used for all calculations and ground-state

*Electrochemical Society Member.
[z]E-mail: liney.arnadottir@oregonstate.edu

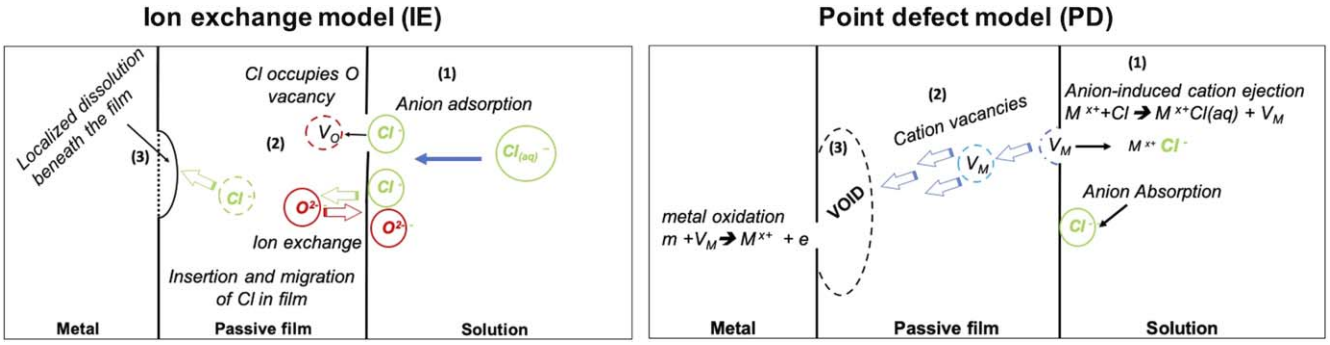

Figure 1. Schematic illustration of the ion exchange model (IE) and the point defect model (PD) describing chloride-induced depassivation mechanism of metals and alloys.[19–22] The numbers (1)–(3) refer to the three stages of the mechanism: For the IE model (1) chloride adsorption; (2) chloride insertion by ion exchange with sub-surface anion or insertion into an O vacancy(V_O) and migration through the oxide and; (3) localized dissolution at the metal/oxide interface. For the PD model (1) surface cation (M^{x+}), in a complex with chloride, ejection from the surface (2) migration of cation vacancy (V_M) to the metal/oxide interface (3) local accumulation of cation vacancies forming a void at the metal/film interface.

configurations were obtained by minimizing total forces on each ion to less than 0.05 eV $Å^{-1}$.

The DFT + U method[38] was used to describe the on-site Coulomb interactions of the localized electrons (3d electrons in Cr). The appropriate U value was determined using ground-state properties including magnetic moment, band gap, and atomic volume for U-J parameters ranging from 0 (GGA limit) to 8 eV, with a constant exchange parameter, J = 1 eV. Figure 2 shows how magnetic moment, band gap, and atomic volume increase with increasing onsite U-J correlations. The magnetic moment and band gap energy remain below the experimental value, whereas the atomic volume is overestimated even at U-J = 0. A U-J value of 4 eV was chosen as an acceptable compromise between structural and electronic properties.

The α-Cr_2O_3 crystal has a hexagonal closed packed array of O atoms with two-thirds of its octahedral interstices occupied by Cr atoms. The α-Cr_2O_3 crystal is antiferromagnetic at ambient conditions with a magnetic structure corresponding to + - + - spin sequence along the [111] axis and overall zero for the slab.[41,42] The adsorption of H_2O and Cl atoms did not affect the magnetic state of the slab. Table I shows the calculated physical properties in comparison with previous studies.

Surface models.—A (2 × 2) α-Cr_2O_3 (0001) cell of six Cr_2O_3 layers (48 Cr atoms and 72 O atoms) and 15 Å vacuum between the periodic slabs in *z-direction* was used for all calculations. The bottom two Cr_2O_3 layers were constrained whereas the remaining

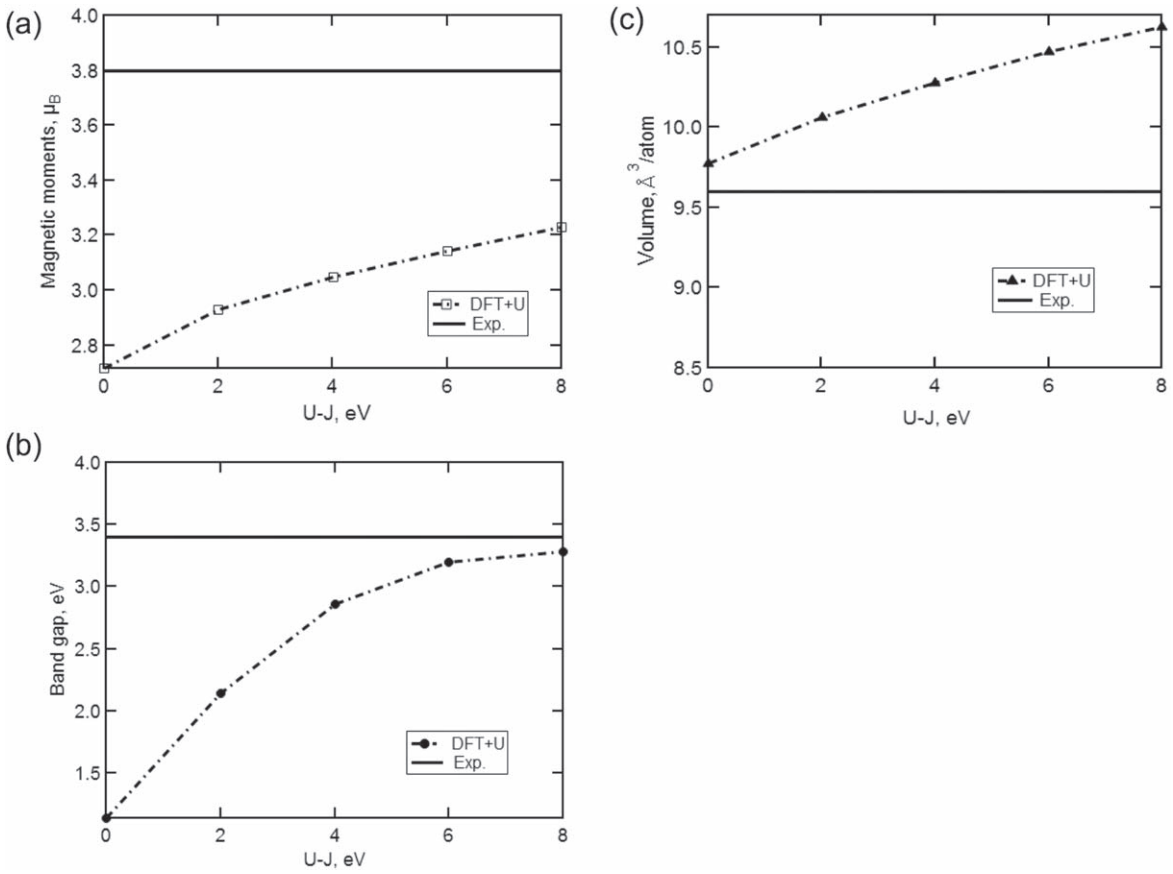

Figure 2. (a) Magnetic moment, (b) band gap, and (c) atomic volume for α-Cr_2O_3 (0001) vs U-J. Experimental values are shown with solid line.[39,40] U-J = 0 represents the GGA limit.

Table I. Physical properties of α-Cr_2O_3.

Properties	This Work	DFT+U[43]	Expt.[40]
Lattice parameter, a (Å)	5.06	5.05	4.95
Lattice parameter, c (Å)	13.92	13.86	13.57
Band gap, (eV)	2.86	2.89	3.40
Magnetic mom, (μ atom^{-1})	3.05	3.10	3.80

layers were allowed to relax. The surface was terminated by four Cr atoms, the most stable surface termination for α-Cr_2O_3 (0001) at low partial pressures of oxygen.[44,45] In aqueous solution, the chlorides are expected to interact with a hydroxylated α-Cr_2O_3 (0001) surface. Costa et al.[46] showed that at ambient conditions, a hydroxylated α-Cr_2O_3 (0001) surface has two H_2O molecules and one OH per surface Cr. Here the hydroxylated surface was made by relaxing a structure starting with three explicit H_2O molecules per Cr to attain the same octahedral coordination of Cr as in the bulk. This structure relaxed to two H_2O and an OH molecule per surface Cr, shown in Fig. 3, consistent with previous studies.[46–49] This surface will be referred to as a hydroxylated surface in the remainder of the paper. The H atom from the dissociated H_2O molecule binds with a subsurface O atom as shown in Fig. 3 (right).

Methodology for studying the degradation mechanism.—The initial step of chloride interaction with a hydroxylated oxide surface for both the ion exchange and the point defect models involves adsorption on the surface which occurs by substitution of OH^- by chlorides on the surface as shown below[23]:

$$M(OH)_x + Cl^- \rightarrow M(OH)_{x-1}Cl + OH^- \quad [1]$$

where reaction 1 describes the substitution of the OH^- on the hydroxylated metal oxide $M(OH)_x$ surface by a chloride forming a metal-chloride-hydroxide ($M(OH)_{x-1}Cl$) complex. This process was modeled by the substitution of H_2O and OH by Cl atoms on the surface following the method of Bouzoubaa et al.[18] This approach has been used by several authors for different metal oxides and alloys[13,18,28,29,48–50] and shown to give the same adsorption trends as chloride and OH^- ions.[51] An energy balance is used to determine the thermodynamic feasibility of the substitution of H_2O and OH by Cl as a function of Cl coverage. Following the substitution, the Cl can go subsurface via insertion into an O vacancy or by an exchange with subsurface OH or O, in accordance with the ion exchange model, or catalyze surface Cr vacancy formation in accordance with the point defect model. Figure 4 shows a schematic of the three mechanisms calculated to determine the thermodynamic feasibility of the different processes: Cl adsorption on the surface by substitution with OH/H_2O, Cl insertion via exchange with subsurface OH or

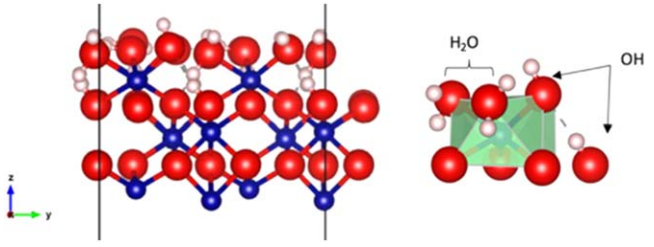

Figure 3. (Left) Side view of the structure of hydroxylated α-Cr_2O_3 (0001) surface. (Right) A coordination polyhedron of a surface Cr atom with O, H_2O and OH species. The Cr is coordinated with three O atoms below the surface and two H_2O molecules, and an OH (from H_2O dissociation) adsorbed on the surface. The H atom from the dissociated H_2O forms an OH with a sub-surface O atom connected to a Cr in an adjacent polyhedron. Red spheres represent O, white spheres represent H, and violet spheres represent Cr.

insertion into an O vacancy (in support of the ion exchange model), and Cl-induced Cr vacancy formation (in support of the point defect model).

Cl surface substitution is expected to begin with H_2O molecules since they are less strongly bonded than the OH species. The substitution energy is calculated according to Eq. 2. A derivation for Eq. 2 is provided in the supplementary information (available online at stacks.iop.org/JES/167/121508/mmedia).

$$\Delta E_{sub} = \frac{\left[(E_{slab/complex} + (m+n)E_{H_2O}) - \left(E_{slab/hydrox} + (m+n)E_{HCl} - \frac{m}{2}E_{H_2}\right)\right]}{(m+n)}, \quad [2]$$

where $complex = (OH)_{4-n}(H_2O)_{8-m}(Cl)_{(m+n)}$

$$hydrox = (OH)_4(H_2O)_8$$

$E_{slab/complex}$ is the total energy of the hydroxylated slab at a given Cl coverage, E_{H_2O} the energy of an isolated water molecule, E_{HCl} the energy of an isolated HCl molecule, $E_{slab/hydrox}$ the total energy of the optimized hydroxylated slab, and E_{H_2} the energy of an isolated H_2 molecule. m and n represent the number of H_2O molecules and OH species substituted by Cl atoms respectively. The energies of the substituted OH species, and Cl atoms were referenced to a H_2O, and HCl, respectively. The substitution energy trends are the same if Cl, and OH are used as reference states.

A Cl monolayer (ML) coverage is defined as the ratio between the number of Cl on the Cr_2O_3 (0001) surface and the maximum number of pre-adsorbed species (OH and H_2O) that could be substituted by Cl, three per Cr atom or 12 for a (2 × 2) cell. The coverage of Cl on the surface is calculated as Eq. 3.

$$\theta = \frac{X_{Cl}}{12} \quad [3]$$

where X_{Cl} is the number of Cl on the studied surface.

The thermodynamic feasibility of Cl insertion via ion exchange with subsurface anion (according to the ion exchange model), was determined by calculating the energy difference between the substituted and the inserted structure as illustrated in Fig. 4b.[5] The insertion energy, ΔE_{insert} was defined according to the Eq. 4:

$$\Delta E_{insert} = E_{slab/ins} - E_{slab/complex} \quad [4]$$

where $E_{slab/ins}$ and $E_{slab/complex}$ represent the total energy of the inserted structure and the total energy of the substituted structure at the same Cl coverage, respectively. A negative insertion energy means that the inserted structure is more stable than the substituted structure suggesting that it is energetically more favorable for the Cl to go into the subsurface than stay on the surface.

The thermodynamic feasibility of Cl-induced cation ejection in the point defect model was determined by calculating the Cr vacancy formation energy, ΔCr_{vac} as a function of Cl coverage. The Cr vacancy formation energy was calculated by comparing the energy of the optimized substituted structure, Fig. 4a, and a defect structure formed by removing a $Cr(OH)_{1-n}(H_2O)_{2-m}(Cl)_{(m+n)}$ complex from the optimized substituted structure leading to the formation of Cr vacancy on the surface, Fig. 4c. The sum of the energy of the optimized defect surface, $E_{slab/vac}$, and the isolated removed complex, $E_{complex}$, was compared with the energy of the structure before the complex removal, $E_{slab/complex}$, expressed as:

$$\Delta E_{Cr_{vac}} = (E_{slab/vac} + E_{complex}) - E_{slab/complex} \quad [5]$$

A positive $\Delta E_{Cr_{vac}}$ value suggests that the removal of the complex, leaving a surface vacancy, is endothermic.

A favorable process corresponds to a negative value (exothermic) for the calculated energy (ΔE_{sub}, ΔE_{insert}, $\Delta E_{Cr_{vac}}$) but an unfavorable

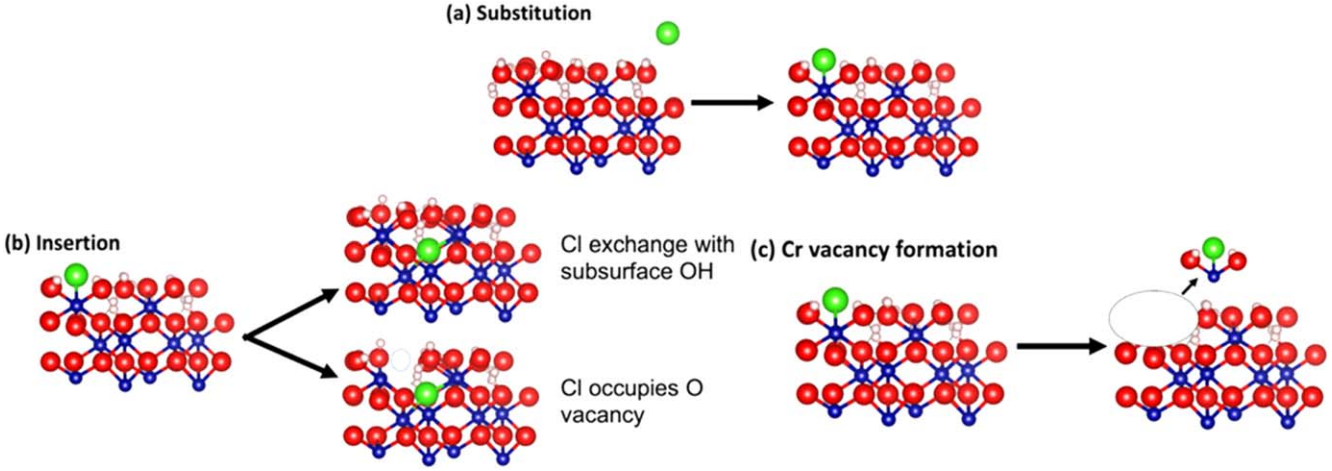

Figure 4. A schematic of the mechanisms calculated herein (a) Cl adsorption by surface substitution of OH/H_2O by Cl, (b) subsurface insertion of Cl by exchange with O/OH or into an O vacancy (according to the ion exchange model) (c) Cl-induced Cr vacancy formation (according to the point defect model). Red spheres represent O, white spheres represent H, violet spheres represent Cr, empty dotted circles represent vacancy and green spheres represent Cl. This color scheme is used throughout this paper.

process corresponds to a positive (endothermic) energy value. More favorable refers to a process trending towards more exothermic (or less endothermic).

Results and Discussion

Energetics of Cl substitution and structural relaxation.—The initial step of chloride interactions with a hydroxylated oxide surface has been suggested to involve competitive adsorption between chlorides and OH^- at the oxide solution interface.[23,52] We examined the thermodynamic feasibility of Cl adsorption, by substitution, on a hydroxylated α-Cr_2O_3 (0001) surface at different Cl coverages up to a monolayer coverage by comparing their substitution energy according to Eq. 2. A monolayer coverage is defined as the highest Cl coverage possible where three Cl atoms interact with each Cr surface atom or a total of 12 Cl in our simulations cell. The substitution energy is plotted as function of Cl coverage and presented in Fig. 5.

The substitution energy is lowest at 2/12 ML but increases with Cl coverage making the substitution less favorable at higher coverage, in good agreement with Cl substitution with OH on hydroxylated NiO (111) surface.[18,53] The increase in substitution energy with coverage is attributed to the increasing electrostatic repulsion between Cl on the surface (see supplementary information).

The substitution also affects the structure of the surface as shown in Fig. 6. The largest changes in the atomic geometry, upon surface relaxation, are in the z-direction and are reported in Fig. 6. From 2/12 ML up to 10/12 ML coverage, the surface structure is split into two layers separated by ~0.7–0.9 Å with the Cl atoms shifted upwards forming the topmost layer whereas the OH/H_2O move downwards to form a second layer. A similar behavior has been shown in hydroxylated NiO(111) surface after Cl substitution.[18] The separation could be ascribed to the variance in ionic radii of Cl (1.75 Å) relative to that of OH (1.10 Å)[54] and H_2O (1.38 Å)[54] leading to misfit constraints and separation of the dissimilar ions to minimize the surface energy. The surface structure at monolayer coverage (12/12 ML) closely resembles the hexavalent Cr atom in the bulk but with longer bonds; Cr–O in the bulk is ~2.05 Å but Cr–Cl on the surface is ~2.40 Å, consistent with Cr–Cl bond length (2.38 A) in $CrCl_3$ salt.[55]

Study of the Cl insertion mechanism in the ion exchange model.—The Cl insertion was studied by the two pathways (see Fig. 4b), exchange with subsurface O/OH or insertions into a subsurface O vacancy.

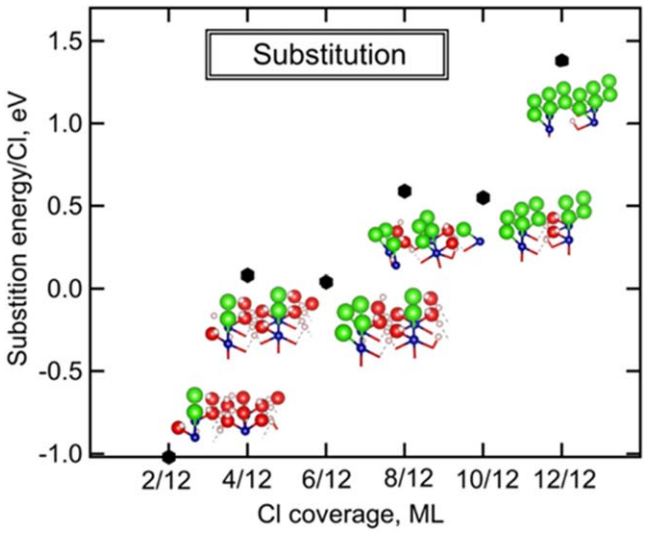

Figure 5. Substitution energy of OH/H_2O substitution by Cl as a function of Cl coverage. At low Cl coverage, Cl substitution is favorable but becomes less favorable with increased Cl coverage.

The feasibility of Cl insertion via ion exchange with subsurface O/OH was determined by the stability of Cl inside the α-Cr_2O_3 layer relative to the surface after the exchange of a surface Cl with an O or OH in the second layer. All non-equivalent sites for Cl insertion, by exchange with O/OH in the second layer, were calculated to determine the lowest energy structure at each coverage. The lowest energy structures for each coverage are presented in Fig. 7. The Cr–OH bond is weaker than the Cr–O bond by 1.5 eV making the Cl insertion via exchange with OH more favorable than an exchange with sub-surface O (from the second layer).

The thermodynamic feasibility of Cl insertion via ion exchange with subsurface OH was determined by the insertion energy according to Eq. 4 and is shown in Fig. 8 as a function of Cl coverage. The insertion energy is a direct comparison of the energy of the inserted and substituted structures, so a negative insertion energy suggests that the inserted structure is more stable than the substituted structure.

The insertion energy is very high and endothermic at low Cl coverage but decreases with increasing Cl coverage. The decreasing insertion energy with increasing Cl coverage can be attributed to the

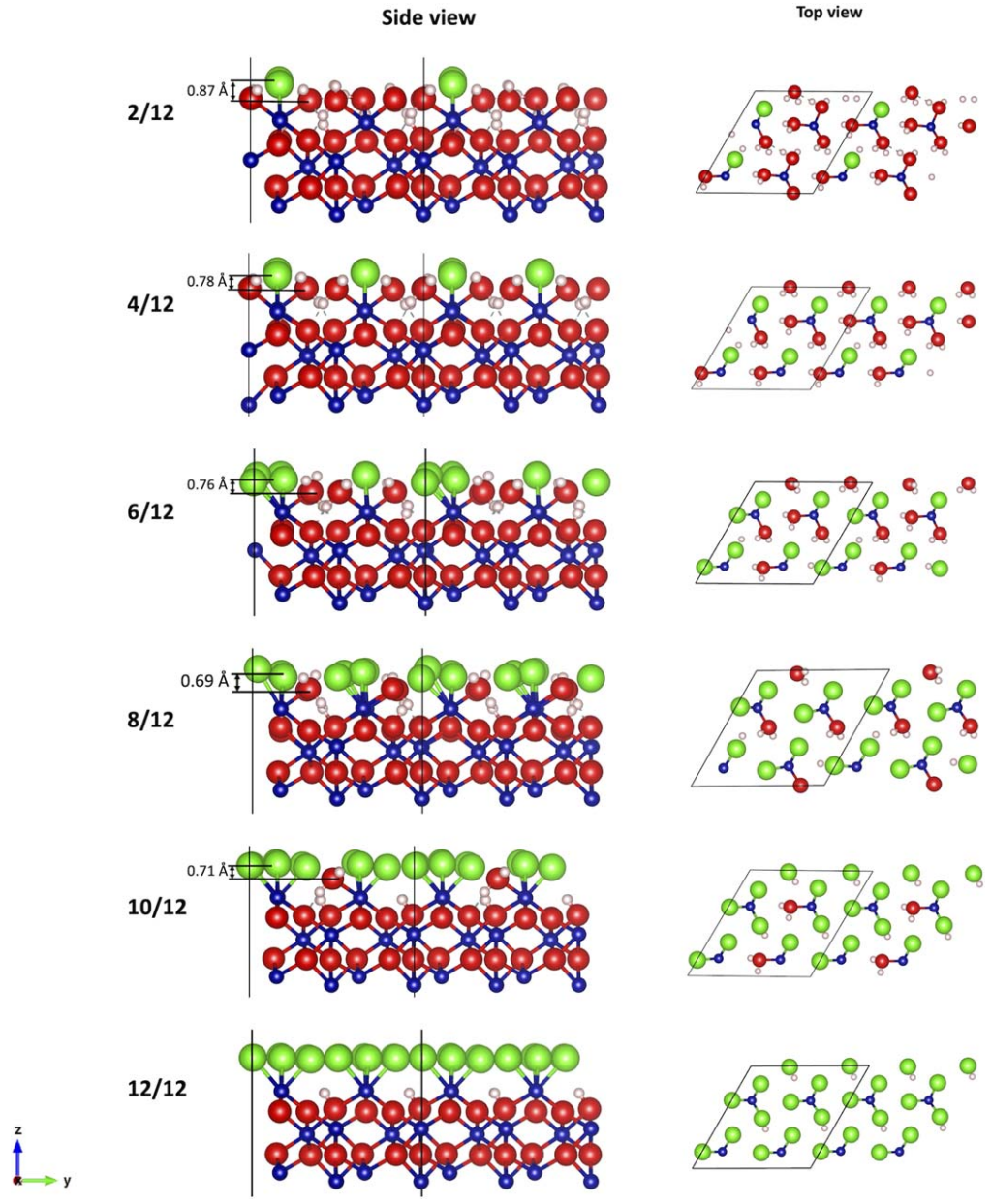

Figure 6. Side (left) and top (right) views of OH/H_2O substituted structures at 2/12–12/12 ML Cl coverage. The average Cl–OH/H_2O distance is indicated on the side view for each coverage. The black lines indicate the boundaries of the simulation cell.

reduction of repulsive interactions between surface Cl atoms after the insertion relative to the substituted structures. At monolayer coverage, Cl insertion energy becomes exothermic suggesting that at full coverage the inserted structure is more favorable than the full coverage substituted structure.

A Cl can also be inserted into the subsurface of the α-Cr_2O_3 layer by occupying an O vacancy. The energy of Cl insertion into an O vacancy was calculated as a function of Cl coverage and is presented in Fig. 9. At the lowest Cl coverage (2/12 ML), the Cl insertion into O vacancy is endothermic, implying an unfavorable process. However, from 4/12 ML Cl coverage and onwards, Cl insertion is exothermic and becomes more negative with increasing coverage. The insertion energy is not reported for the monolayer coverage because the "initial state" is not stable but relaxes to a final state with Cl in the subsurface O vacancy.

The insertion of Cl also affects the surface structure (Fig. 7) and the Cl-OH/H_2O interlayer distance but the effect is smaller for the inserted structures, ∼0.5–∼0.8 Å compared to ∼0.7–0.9 Å for the surface substituted structures. An inserted Cl, by exchange with OH, also affects the Cr atoms in the first layer to which they are connected by shifting it upward by approximately ∼0.1–0.3 Å and reducing the interaction between the surface Cr and the rest of the bulk.

Effect of inserted Cl on further Cl insertion.—Calculations were done to determine whether an already inserted Cl (pre-inserted Cl) enhances additional Cl insertion into subsurface O vacancies as described in Fig. 10. Four cases were examined varying the distance between the pre-inserted subsurface Cl (dark green) and the O vacancy (black dashed circle). Case D has no pre-inserted Cl atoms and serves as a reference where the pre-inserted subsurface Cl is infinitely far away. The calculations were done at (2/12) ML Cl coverage. Figure 10 shows the insertion energy of Cl into an O vacancy with the pre-inserted Cl at different depths from the surface (A-C) and without any pre-inserted Cl (D). The insertion energy was lowest when the pre-inserted Cl atom was closest to the O vacancy (case A) and increased with increasing distance between the

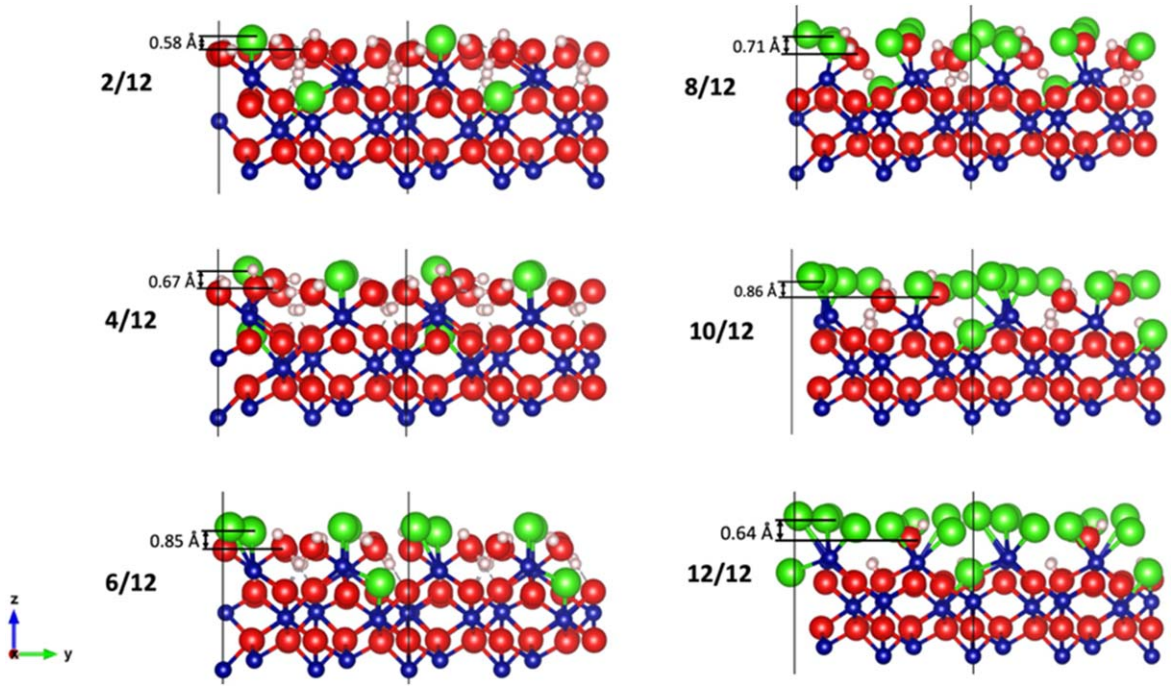

Figure 7. Side views of structures with one Cl inserted at 2/12–12/12 ML Cl coverage. The average Cl–OH/H_2O distance at the surface is indicated on the left side of the figure. The black lines indicate the periodic boundaries of the simulation cell.

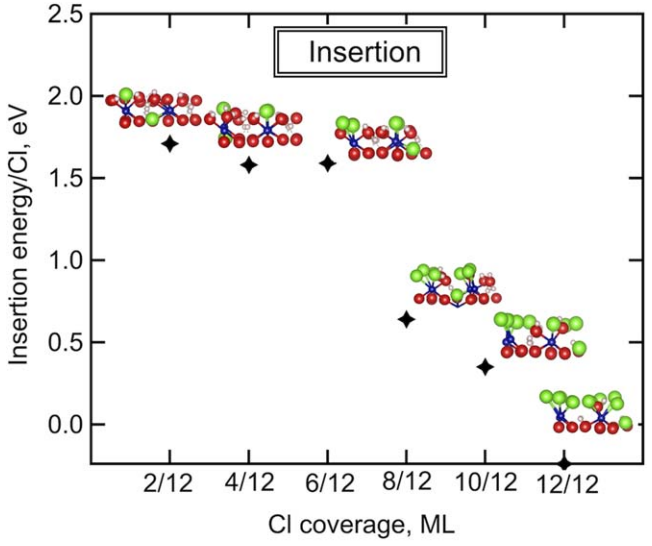

Figure 8. The Cl insertion energy by ion exchange with (subsurface) OH as a function of Cl coverage. Cl insertion is unfavorable at low coverage but becomes more favorable with increased Cl coverage. At full coverage, the Cl insertion energy is exothermic.

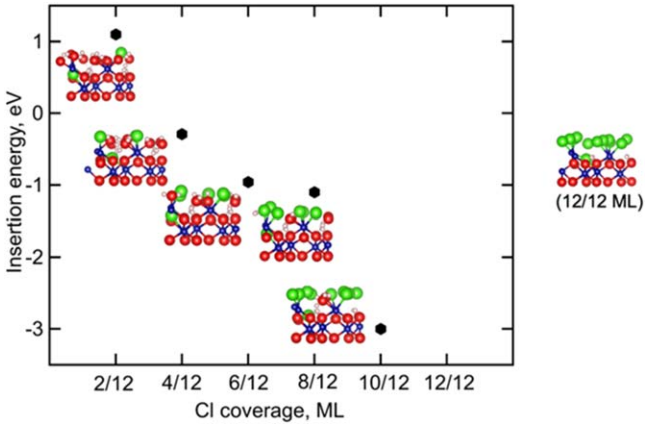

Figure 9. The energy of Cl insertion into an oxygen subsurface vacancy as a function of Cl coverage. Cl insertion is exothermic from 4/12 ML coverage onward. The insertion energy at full coverage (12/12 ML) is not included because the structure relaxes to a configuration with Cl in the subsurface O vacancy, so no energy difference could be calculated. A figure of the 12/12 ML structure is shown on right.

pre-inserted Cl and the O vacancy. This shows that pre-inserted Cl can help facilitate additional Cl insertion into the oxygen vacancies. This is comparable to observation by Liu et al.[13] for pre-inserted Cl in Al_2O_3 passive layer.

Study of the Cr vacancy formation according to the point defect model.—The energetics of surface Cr vacancy formation, a crucial step in the point defect model was investigated by calculating the Cl-induced chromium vacancy formation on the surface. Figure 11 shows the Cr vacancy formation energy as a function of the Cl coverage. A negative Cr vacancy formation energy suggests that it is more favorable to separate the $Cr(OH)_n(H_2O)_m(Cl)_{(m+n)}$ complex from the surface, forming a Cr vacancy, than to be on the surface. Cr vacancy formation is least favorable at the lowest Cl coverage but becomes more favorable with increasing Cl coverage. From 10/12 ML Cl coverage onward, Cr vacancy formation energy is negative (exothermic process) which implies the structure is more stable without the $CrCl_3$ on the surface. This means that at high Cl coverage, the $CrCl_3$ formed on the surface favors removal to create a vacancy on the surface. The favorability of Cl-induced Cr removal at high coverages is consistent with the critical Cl threshold concept which has been widely demonstrated through electrochemical studies.[56–58] Our findings also agree with the effect of high local Cl coverage on the chloride-induced surface Fe vacancy formation on Fe_2O_3 by DorMohammadi et al.[24] and Pang et al.[29]

This suggests that the Cr vacancy formation step of the point defect model, like Cl insertion, is a coverage driven process where at high coverages, the removal of the $CrCl_3$ from the α-Cr_2O_3 surface is favored.

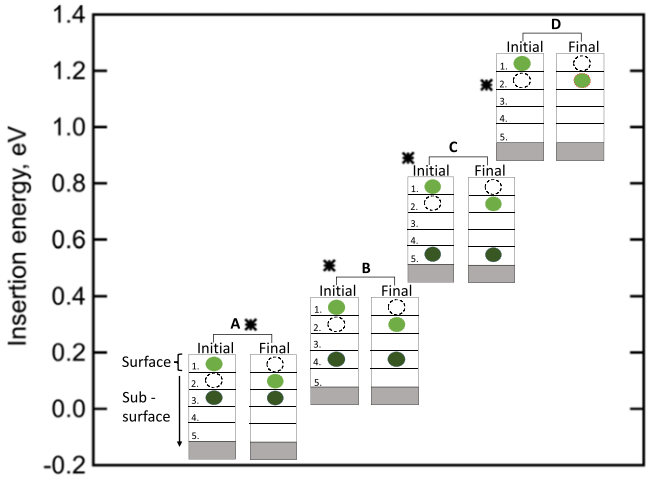

Figure 10. Insertion energy for Cl inserted from the surface (green filled circle) into a neighboring subsurface O vacancy (black dashed circle) with pre-inserted Cl (dark-green filled circle) at different depths from the surface (A-C) and no pre-inserted Cl (D). Figure insets schematically show the initial and the final state of insertion. Cases with more positive insertion energy are thermodynamically less favored.

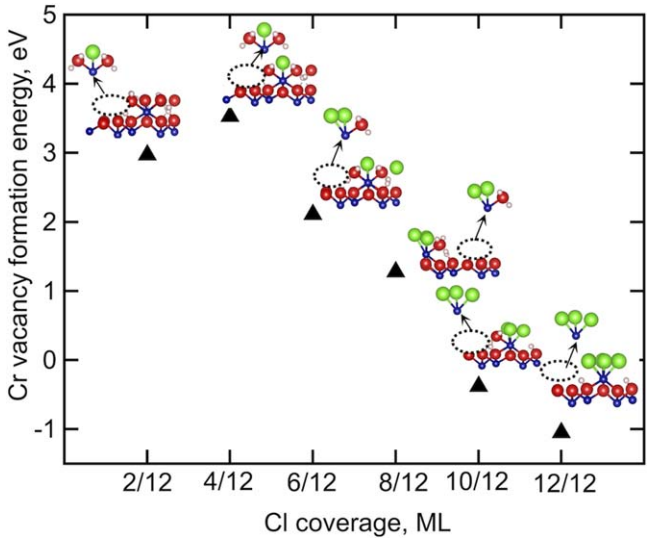

Figure 11. Cr vacancy formation energy as a function of Cl coverage on the substituted structure. Negative (positive) energy values correspond to exothermic (endothermic) process.

Cr vacancy formation after Cl insertion.—The insertion of Cl into the second layer leads to structural changes that can result in the formation of a Cr vacancy on the surface. An example of the structural changes is presented for a monolayer coverage in Fig. 12a where inserted Cl interacts directly with Cr1 in Fig. 12 pushing it upward by 0.3 Å relative to the other surface Cr atoms (labeled Cr2 in Fig. 12) not bonded to the inserted Cl atom. Figure 12b shows a graph of the Cr vacancy formation energy as a function of Cl coverage. At low Cl coverage, Cr vacancy formation after Cl insertion is unfavorable, but it becomes more favorable with increasing Cl coverage and exothermic at full coverage. This suggests that Cr vacancies can be formed after Cl insertion at full coverage.

Implications for the point defect and ion exchange degradation models.—We used DFT to investigate critical steps of two common passive layer degradation models: ion exchange model and the point defect model on a hydroxylated α-Cr_2O_3(0001) surface. Both models begin with Cl adsorption by substitution with OH and H_2O species on the surface. We found that at the lowest Cl coverages, Cl substitution with surface H_2O/OH was favorable but became less favorable with increasing Cl coverage.

Cl insertion via ion exchange or into an oxygen vacancy (see Figs. 1 and 4b) is an integral part of the ion exchange model. At lower Cl coverages, Cl insertion by exchange with subsurface OH was unfavorable while at higher Cl coverage, Cl insertion was favorable. Cl insertion into O vacancy near the surface was thermodynamically feasible (exothermic) except at the lowest coverage (2/12 ML) and it becomes more exothermic with increasing coverage. This suggests that the presence of an O vacancy near the surface of the α-Cr_2O_3(0001) can facilitate the insertion of Cl into the oxide even at lower coverages. The stability of Cl in the subsurface of the film is consistent with experimental observations of chloride inside the Cr_2O_3 passive films exposed to high chloride concentration environments.[15,16] This implies that the Cl insertion step described by the ion exchange model for α-Cr_2O_3 degradation would be feasible at a full Cl coverage and even at relatively lower coverages for surfaces with oxygen vacancies. An inserted Cl was also found to promote additional Cl insertions into O vacancies close to the surface.

The initial stages of the point defect model were analyzed by the Cl-induced Cr vacancy formation. In the absence of Cl, Cr vacancy formation was very unfavorable; however, Cr vacancy formation became more favorable with higher Cl coverage and exothermic at the highest ($\geqslant$10/12 ML) coverages. This suggests that the critical Cr vacancy formation step in the point defect model is thermodynamically feasible at high surface Cl concentrations in good agreement with DFT studies on Fe_2O_3.[29] Cr vacancy formation was also found to be favorable at full coverage with the inserted Cl in the subsurface (according to the ion exchange model).

This suggests that the initial stages of Cl-induced degradation of the Cr_2O_3 passive layer may involve a complex combination of the point defect and the ion exchange models which depends on Cl coverage and the presence of O vacancies near the surface.

An O vacancy near the surface can facilitate Cl insertion into the subsurface even at low Cl coverages ($\geqslant$4/12 ML) making the ion exchange model the likely mechanism, while in the absence of an O vacancy, both Cl insertion and Cr vacancy formation are endothermic at low Cl coverages.

At high coverages, Cl induced Cr vacancy formation, in support of the point defect model, becomes thermodynamically feasible at 10/12 ML and above, while the Cl insertions only becomes exothermic at 12/12 ML. This suggests that at higher coverages, the Cl-induced degradations are first activated through a vacancy formation mechanism but both insertion and vacancy formation would be feasible at the full coverage. The effects of structural defects, such as step edges, have been shown to significantly contribute to the degradation of the passive layer[59,60] but these were not considered herein.

Conclusions

DFT calculations were used to compare the thermodynamic feasibility of critical steps in the ion exchange and point defect models of Cl enhanced degradation of α-Cr_2O_3.

Both models start with Cl substitution with H_2O/OH which was found to be favorable at low Cl coverages but unfavorable at high Cl coverages. For the ion exchange model, Cl insertion by exchange with OH was unfavorable at low Cl coverage but favorable at full Cl coverage, whereas insertion into a neighboring O subsurface vacancy was exothermic except, at the lowest Cl coverage of 2/12 ML. The presence of an inserted Cl near subsurface oxygen vacancies facilitated the insertion of additional Cl.

The Cl-induced Cr vacancy formation is unfavorable at low Cl coverage but favorable at high Cl ($\geqslant$10/12 ML) coverage in good agreement with the key hypothesis of the point defect model where Cl acts as a catalyst in the degradation process by inducing the formation of cation vacancies on the surface. With the insertion of Cl, the Cr atom bonded to the Cl in the subsurface favored removal from the surface only at full coverage.

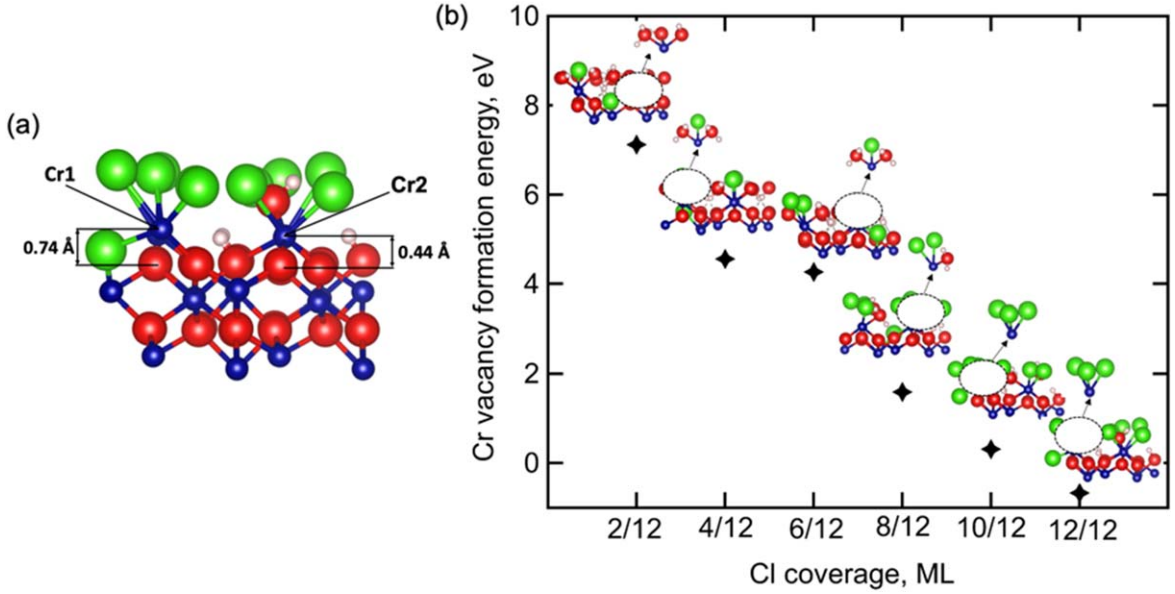

Figure 12. (a) Side view of an inserted structure at 12/12 ML showing the distance between the Cr atom connected to the inserted Cl (labeled as Cr1) and the Cr not connected to the inserted Cl (Cr2). (b) the Cr-vacancy formation energy for surface Cr bonded to the inserted Cl as a function of Cl coverage. Cr vacancy formation after insertion is only exothermic at full Cl coverage (12/12 ML).

Our findings suggest that the initial stages of the degradation of the hydroxylated Cr passive layer depend on Cl coverage and the presence of O vacancy near the surface. Cl insertion (in support of the ion exchange model) is thermodynamically feasible in the presence of O vacancies even at low coverages but neither insertion nor Cr vacancy formation is feasible in the absence of O vacancies at low coverages. Cr vacancy formation (in support of the point defect model) is first activated at higher coverages because it becomes feasible from 10/12 ML onwards whereas Cl insertion by exchange with subsurface OH (in support of the ion exchange model) only becomes feasible at full coverage.

Acknowledgments

This research is supported by the U.S. Department of Energy, Nuclear Energy University programs under the grant DE-NE0008668. Part of the calculations used the Extreme Science and Engineering Discovery Environment (XSEDE)[61] (allocations TG-DMR160093 and TG-ENG170002) which is supported by National Science Foundation grant number ACI-1053575. The authors acknowledge the Texas Advanced Computing Center (TACC) at the University of Texas at Austin and the Comet cluster at the San Diego Supercomputer Center, and the High-Performance Computing (HPC) center at Idaho National Laboratory for providing HPC resources that have contributed to the research results reported within this paper. K.O Sarfo acknowledges the Idaho National Laboratory summer internship program.

ORCID

Kofi Oware Sarfo https://orcid.org/0000-0002-4426-1582
Pratik Murkute https://orcid.org/0000-0002-7863-6346
O. Burkan Isgor https://orcid.org/0000-0002-0554-3501
Yongfeng Zhang https://orcid.org/0000-0003-2730-3549
Julie Tucker https://orcid.org/0000-0002-0886-1580
Líney Árnadóttir https://orcid.org/0000-0001-9013-4173

References

1. J. E. Tang, M. Halvarsson, H. Asteman, and J. E. Svensson, "Microstructure of oxidised 304L steel and the effects of surface roughness on oxidation behaviour." *Mater. Sci. Forum*, **369–372**, 205 (2001).
2. R. Kirchheim, B. Heine, H. Fischmeister, S. Hofmann, H. Knote, and U. Stolz, "The passivity of iron-chromium alloys." *Corros. Sci.*, **29**, 899 (1989).
3. A. Fossati, F. Borgioli, E. Galvanetto, and T. Bacci, "Corrosion resistance properties of glow-discharge nitrided AISI 316L austenitic stainless steel in NaCl solutions." *Corros. Sci.*, **48**, 1513 (2006).
4. P. Cao, D. Wells, and M. P. Short, "Anisotropic ion diffusion in α-Cr_2O_3: an atomistic simulation study." *Phys. Chem. Chem. Phys.*, **19**, 13658 (2017).
5. E. McCafferty, "Sequence of steps in the pitting of aluminum by chloride ions." *Corros. Sci.*, **45**, 1421 (2003).
6. B. MacDougall, "Incorporation of chloride ion in passive oxide films on nickel." *J. Electrochem. Soc.*, **130**, 543 (1983).
7. O. J. Murphy, "Chloride ion penetration of passive films on iron." *J. Electrochem. Soc.*, **130**, 1792 (1983).
8. P. Marcus and J. M. Herbelin, "The entry of chloride ions into passive films on nickel studied by spectroscopic (ESCA) and nuclear (36Cl radiotracer) methods." *Corros. Sci.*, **34**, 1123 (1993).
9. P. M. Natishan, W. E. O'Grady, F. J. Martin, R. J. Rayne, H. Kahn, and A. H. Heuer, "Chloride interactions with the passive films on stainless steel." *J. Electrochem. Soc.*, **158**, C7 (2011).
10. W. Khalil, S. Haupt, and H.-H. Strehblow, "The thinning of the passive layer of iron by halides." *Mater. Corros.*, **36**, 16 (1985).
11. E. McCafferty, "The electrode kinetics of pit initiation on aluminum." *Corros. Sci.*, **37**, 481 (1995).
12. S. Y. Yu, W. E. O'Grady, D. E. Ramaker, and P. M. Natishan, "Chloride ingress into aluminum prior to pitting corrosion an investigation by XANES and XPS." *J. Electrochem. Soc.*, **147**, 2952 (2000).
13. M. Liu, Y. Jin, C. Leygraf, and J. Pan, "A DFT-Study of Cl Ingress into α-Al_2O_3(0001) and Al(111) and its possible influence on localized corrosion of Al." *J. Electrochem. Soc.*, **166**, C3124 (2019).
14. B. Zhang, J. Wang, B. Wu, X. W. Guo, Y. J. Wang, D. Chen, Y. C. Zhang, K. Du, E. E. Oguzie, and X. L. Ma, "Unmasking chloride attack on the passive film of metals." *Nat. Commun.*, **9**, 2559 (2018).
15. S. Deng, S. Wang, L. Wang, J. Liu, and Y. Wang, "Influence of chloride on passive film chemistry of 304 stainless steel in sulphuric acid solution by glow discharge optical emission spectrometry analysis." *Int. J. Electrochem. Sci.*, **12**, 1106 (2017).
16. S. A. Saadi, Y. Yi, P. Cho, C. Jang, and P. Beeley, "Passivity breakdown of 316L stainless steel during potentiodynamic polarization in NaCl solution." *Corros. Sci.*, **111**, 720 (2016).
17. S. Zhang, Z. Wang, X. Chang, W. Hou, and J. Wang, "Identifying the role of nanoscale heterogeneities in pitting behaviour of Al-based metallic glass." *Corros. Sci.*, **53**, 3007 (2011).
18. A. Bouzoubaa, B. Diawara, V. Maurice, C. Minot, and P. Marcus, "Ab initio study of the interaction of chlorides with defect-free hydroxylated NiO surfaces." *Corros. Sci.*, **51**, 941 (2009).
19. D. D. Macdonald, "The point defect model for the passive state." *J. Electrochem. Soc.*, **139**, 3434 (1992).
20. J. Soltis, "Passivity breakdown, pit initiation and propagation of pits in metallic materials—review." *Corros. Sci.*, **90**, 5 (2015).
21. M. Urquidi, "Solute-vacancy interaction model and the effect of minor alloying elements on the initiation of pitting corrosion." *J. Electrochem. Soc.*, **132**, 555 (1985).
22. M. Heine, D. Keir, and M. Pryor, "The specific effects of chloride and sulfate ions on oxide covered aluminum." *J. Electrochem. Soc.*, **112**, 24 (1965).

23. Z. A. Foroulis and M. J. Thubrikar, "On the kinetics of the breakdown of passivity of preanodized aluminum by chloride ions." *J. Electrochem. Soc.*, **122**, 1296 (1975).
24. H. DorMohammadi, Q. Pang, P. Murkute, L. Árnadóttir, and O. B. Isgor, "Investigation of chloride-induced depassivation of iron in alkaline media by reactive force field molecular dynamics." *npj Materials Degradation*, **3**, 19 (2019).
25. Y. Zhao and W. Jin, "Chapter 2 - Steel corrosion in concrete." *Steel Corrosion-Induced Concrete Cracking*, ed. Y. Zhao and W. Jin (Butterworth-Heinemann imprint of Elsevier, Oxford, United Kingdom) p. 19 (2016).
26. A. Bouzoubaa, B. Diawara, V. Maurice, C. Minot, and P. Marcus, "Ab initio modelling of localized corrosion: study of the role of surface steps in the interaction of chlorides with passivated nickel surfaces." *Corros. Sci.*, **51**, 2174 (2009).
27. H. DorMohammadi, Q. Pang, L. Árnadóttir, and O. Burkan Isgor, "Atomistic simulation of initial stages of iron corrosion in pure water using reactive molecular dynamics." *Comput. Mater. Sci.*, **145**, 126 (2018).
28. Q. Pang, H. DorMohammadi, O. B. Isgor, and L. Árnadóttir, "Density functional theory study on the effect of OH and Cl adsorption on the surface structure of α-Fe2O3." *Computational and Theoretical Chemistry*, **1100**, 91 (2017).
29. Q. Pang, H. DorMohammadi, O. B. Isgor, and L. Árnadóttir, "The effect of surface vacancies on the interactions of Cl with a α-Fe2O3 (0001) surface and the role of Cl in depassivation." *Corros. Sci.*, **154**, 61 (2019).
30. M. Liu, Y. Jin, C. Zhang, C. Leygraf, and L. Wen, "Density-functional theory investigation of Al pitting corrosion in electrolyte containing chloride ions." *Appl. Surf. Sci.*, **357**, 2028 (2015).
31. G. Kresse and J. Furthmüller, "Efficient iterative schemes for ab initio total-energy calculations using a plane-wave basis set." *Physical Review B*, **54**, 11169 (1996).
32. G. Kresse and J. Furthmüller, "Efficiency of ab-initio total energy calculations for metals and semiconductors using a plane-wave basis set." *Comput. Mater. Sci.*, **6**, 15 (1996).
33. G. Kresse and J. Hafner, "Ab initio molecular dynamics for liquid metals." *Physical Review B*, **47**, 558 (1993).
34. G. Kresse and J. Hafner, "Ab initio molecular-dynamics simulation of the liquid-metal–amorphous-semiconductor transition in germanium." *Physical Review B*, **49**, 14251 (1994).
35. J. P. Perdew, K. Burke, and M. Ernzerhof, "Generalized gradient approximation made simple." *Phys. Rev. Lett.*, **77**, 3865 (1996).
36. G. Kresse and D. Joubert, "From ultrasoft pseudopotentials to the projector augmented-wave method." *Physical Review B*, **59**, 1758 (1999).
37. P. E. Blöchl, "Projector augmented-wave method." *Physical Review B*, **50**, 17953 (1994).
38. S. L. Dudarev, G. A. Botton, S. Y. Savrasov, C. J. Humphreys, and A. P. Sutton, "Electron-energy-loss spectra and the structural stability of nickel oxide: an LSDA +U study." *Physical Review B*, **57**, 1505 (1998).
39. L. Pauling and S. B. Hendricks, "The crystal structures of hematite and corundum." *Journal of the American Chemical Society*, **47**, 781 (1925).
40. L. W. Finger and R. M. Hazen, "Crystal structure and isothermal compression of Fe_2O_3, Cr_2O_3, and V_2O_3 to 50 kbars." *J. Appl. Phys.*, **51**, 5362 (1980).
41. T. G. Worlton, R. M. Brugger, and R. B. Bennion, "Pressure dependence of the Néel temperature of Cr_2O_3." *J. Phys. Chem. Solids*, **29**, 435 (1968).
42. R. H. Bruce and D. S. Cannell, "Specific heat of Cr_2O_3 near the Néel temperature." *Physical Review B*, **15**, 4451 (1977).
43. C. Gray, Y. Lei, and G. Wang, "Charged vacancy diffusion in chromium oxide crystal: DFT and DFT+U predictions." *J. Appl. Phys.*, **120**, 215101 (2016).
44. A. Rohrbach, J. Hafner, and G. Kresse, "Ab initio study of the (0001) surfaces of hematite and chromia: influence of strong electronic correlations." *Physical Review B*, **70**, 125426 (2004).
45. V. Maurice, S. Cadot, and P. Marcus, "XPS, LEED and STM study of thin oxide films formed on Cr(110)." *Surf. Sci.*, **458**, 195 (2000).
46. D. Costa, K. Sharkas, M. M. Islam, and P. Marcus, "Ab initio study of the chemical states of water on Cr_2O_3(0001): from the isolated molecule to saturation coverage." *Surf. Sci.*, **603**, 2484 (2009).
47. M. A. Henderson and S. A. Chambers, "HREELS, TPD and XPS study of the interaction of water with the α-Cr_2O_3(001) surface." *Surf. Sci.*, **449**, 135 (2000).
48. B. Diawara, A. Bouzoubaa, N. Pineau, C. Minot, V. Maurice, and P. Marcus, "DFT study of the interactions of Cl^- with passivated Nickel surfaces: energetic and structural aspects." *Passivation of Metals and Semiconductors, and Properties of Thin Oxide Layers* in, ed. P. Marcus and V. Maurice (Elsevier Science, Amsterdam) p. 659 (2006).
49. K. N. Nigussa, Ø. Borck, and J. A. Støvneng, "Adsorption of H2S on α-Cr_2O_3(0001) surfaces: a density functional theory investigation." *Corros. Sci.*, **111**, 1 (2016).
50. K. N. Nigussa, K. L. Nielsen, Ø. Borck, and J. A. Støvneng, "Adsorption of hydrogen, chlorine, and sulfur atoms on α-Cr_2O_3(0001) surfaces: a density functional theory investigation." *Corros. Sci.*, **53**, 3612 (2011).
51. A. M. Pessoa, J. L. C. Fajín, J. R. B. Gomes, and M. N. D. S. Cordeiro, "Ionic and radical adsorption on the Au(hkl) surfaces: a DFT study." *Surf. Sci.*, **606**, 69 (2012).
52. H. H. Strehblow, "Nucleation and repassivation of corrosion pits for pitting on iron and nickel." *Mater. Corros.*, **27**, 792 (1976).
53. N. Pineau, C. Minot, V. Maurice, and P. Marcus, "Density functional theory study of the interaction of Cl − with passivated nickel surfaces." *Electrochem. Solid-State Lett.*, **6**, B47 (2003).
54. Y. Marcus, "Volumes of aqueous hydrogen and hydroxide ions at 0 to 200 °C." *J. Chem. Phys.*, **137**, 154501 (2012).
55. C. L. Rollinson, *The Chemistry of Chromium, Molybdenum and Tungsten: Pergamon International Library of Science, Technology, Engineering and Social Studies* (Elsevier, Amsterdam) (2015).
56. U. M. Angst, B. Elsener, C. K. Larsen, and Ø. Vennesland, "Chloride induced reinforcement corrosion: electrochemical monitoring of initiation stage and chloride threshold values." *Corros. Sci.*, **53**, 1451 (2011).
57. P. Ghods, O. B. Isgor, G. A. McRae, and G. P. Gu, "Electrochemical investigation of chloride-induced depassivation of black steel rebar under simulated service conditions." *Corros. Sci.*, **52**, 1649 (2010).
58. U. Angst, B. Elsener, C. K. Larsen, and Ø. Vennesland, "Critical chloride content in reinforced concrete—a review." *Cem. Concr. Res.*, **39**, 1122 (2009).
59. V. Maurice and P. Marcus, "Progress in corrosion science at atomic and nanometric scales." *Prog. Mater Sci.*, **95**, 132 (2018).
60. O. M. Magnussen, L. Zitzler, B. Gleich, M. R. Vogt, and R. J. Behm, "In-situ atomic-scale studies of the mechanisms and dynamics of metal dissolution by high-speed STM." *Electrochim. Acta*, **46**, 3725 (2001).
61. J. Towns et al., "XSEDE: accelerating scientific discovery." *Computing in Science & Engineering*, **16**, 62 (2014).